



How can we trust TROPOMI based Methane Emissions Estimation: Calculating Emissions over Unidentified Source Regions

Bo Zheng^{1,2}, Jason Blake Cohen^{1,2*}, Lingxiao Lu^{1,2}, Wei Hu^{1,2}, Pravash Tiwari^{1,2}, Simone Lolli³, Andrea Garzelli⁴, Hui Su⁵, Kai Qin^{1,2*}

¹School of Environment and Spatial Informatics, China University of Mining and Technology, Xuzhou 221116, China

²Shanxi Key Laboratory of Environmental Remote Sensing Applications, China University of Mining and Technology, Xuzhou 221116, China

³CNR-Institute of Methodologies for Environmental Analysis (IMAA), Contrada S. Loja, Tito Scalco, 85050, Italy

10 ⁴Department of Information Engineering and Mathematics, University of Siena, 53100 Siena, Italy

⁵Department of Civil and Environmental Engineering, Space Science and Technology Institute, The Hong Kong University of Science and Technology, Clear Water Bay, Hong Kong SAR

Correspondence to: Jason B. Cohen and Kai Qin (jasonbc@alum.mit.edu ; jasonbc@cumt.edu.cn ; qinkai@cumt.edu.cn)

Abstract. We propose a novel method for computing the effects of TROPOMI observational uncertainties on emissions calculation arising from the nonlinearity of the gradient terms and non-biased filtering in space and time. Application using TROPOMI XCH₄ data in clean areas of Western China with long-term WMO background observations quantifies a minimum detectable emission threshold of 1.8 µg/m²/s, lower than existing community thresholds using TROPOMI. By combining threshold-based and stochastic approaches that incorporates pixel-by-pixel and day-by-day XCH₄ uncertainties, we identify and filter physically unrealistic emission values in both space and time. The resulting emissions reveal both missing sources and a 5% emission bias caused by the nonlinearity of the gradient term. Validation was performed by applying the method to the Permian Basin, where comparisons with airborne observations demonstrate the method's ability to align with independent datasets. The importance and implications of our results are related to this being a new methodology for methane emissions estimate from TROPOMI which enables precise identification of emission sources and improved handling of observational noise, offering a more accurate framework for methane emission monitoring across diverse regions using existing satellite platforms. Our results yield a non-negative emissions dataset using an objective selection and filtration method, which includes a lower minimum emissions threshold on all grids and reduction of false positives. Finally, the new approach can be adopted to other satellite platforms to provide a more robust and reliable quantification of emissions under data uncertainty that moves beyond traditional plume identification and background subtraction.



1 Introduction

Methane (CH_4) is a potent greenhouse gas with a global warming potential (GWP) estimated to be 28-34 times that of carbon dioxide over a 100-year period and 84-87 times on a 20-year time scale (Hu et al., 2024; Vanselow et al., 2024; Liang et al., 2023). Major sources of methane include fossil fuel extraction, agricultural activities (such as rice paddies and livestock), waste disposal, and wetlands (Vanselow et al., 2024). Since the start of the Industrial Revolution, methane concentrations have been observed to significantly increase (Liang et al., 2023; Erland et al., 2022), with periods of both larger growth and slower or no growth contained within, contributing significantly to the present amount of observed surface warming (Vanselow et al., 2024; Erland et al., 2022; Prinn et al., 2001). Due to its relatively shorter atmospheric lifetime compared with many other greenhouse gasses, accurately quantifying and controlling methane emissions is crucial in addressing global warming in the near-term (Erland et al., 2022; Liu, J et al., 2024b).

In recent years, with the development of satellite remote sensing technology, various platforms from space have become more relevant at aiding the monitoring of methane concentrations in the atmosphere (Gao et al., 2023; Nesser et al., 2024). Among them, TROPOMI, GOSAT and SCIAMACHY have been used for its retrieval of a physical atmospheric CH_4 column retrieval (XCH_4), allowing indirect validation by surface networks (i.e., AGAGE and WMO) as well as upward looking surface observational networks (i.e., TCOON) (Hu et al., 2016; Parker et al., 2011; Frankenberg et al., 2005). TROPOMI in particular offers a combination of daily XCH_4 retrieval, global coverage, and high spatial resolution (Erland et al., 2022; Liu, M et al., 2024; Gao et al., 2023; Nesser et al., 2024; Hu et al., 2016). Due to its extensive use to monitor other atmospheric constituents impacting air pollution, there is extensive work on the uncertainty of TROPOMI products including: NO_2 from 10% to 40% (Boersma et al., 2018; Pollard et al., 2022), black carbon aerosol (BC) from 20%-50% (Vignati et al., 2010; Tiwari et al., 2023, 2025), and CO starting from a minimum of 10% to 20% and upwards, without a well-defined upper range (Sha et al., 2021). Additionally, XCH_4 from this platform has a significant number of pixels with missing data (Schneising et al., 2023; Qu et al., 2021; Hachmeister et al., 2022; Frankenberg et al., 2016; Hu et al., 2018). Therefore, XCH_4 is expected to also have a significant uncertainty, due to at least the following factors: sensor and waveband resolution issues (Hu et al., 2018), atmospheric conditions which reduce the already relatively weak incoming shortwave infrared radiation such as clouds and aerosols (Balasus et al., 2023; Liu, Z et al., 2024; Liu, J et al., 2024a), and surface reflectivity (Balasus et al., 2023).

Computing emissions from concentration requires an additional step that includes knowledge of the wind, atmospheric transport and diffusion, in-situ processing and other processes (Cohen and Prinn 2011; Cohen et al., 2011). There are many studies which have used various complex and simple models to attempt to estimate emissions from TROPOMI in near real time for various species (Hu et al., 2024; Qin et al., 2023; Liu, J et al., 2024b; Cohen et al., 2025; Li et al., 2023). However, due to the uncertainties in the retrieved TROPOMI data and wind fields, the computation of gradient term(s) necessary to compute emissions may lead to significant non-linearity (Cohen and Prinn 2011; Cohen et al., 2011; He et al., 2024). Therefore, finding ways to address how observed and modeled uncertainties lead to the robustness of inverted methane



emissions is a necessary and essential step to gain trust in resulting emission quantification and usefulness for attribution (Cohen et al., 2025; Tiwari et al., 2025). To gain confidence, such emissions should include methods which are both unbiased and robust, and are capable of identifying sources both known and unknown, monitoring emissions from those sources, and validate whether emissions are actually being reduced or eliminated (Hemati et al., 2024).

In this study, we quantify CH₄ emissions in a clean area with a long-term WMO observational station (Waliguan) using a flexible mass-conserving method that explicitly accounts for the impacts of XCH₄ observational uncertainties on the gradient terms and their influence on emission inversion. Selecting a region devoid of large emission sources is critical, as it allows for an objective demonstration of the effects of white noise generated by the nonlinearity of the gradient term on emission calculations. To address this, we introduce unbiased thresholds and filters to systematically separate genuine emission signals from white noise, effectively eliminating physically implausible emission values in an unbiased manner. Our results demonstrate that all identified emissions correspond to spatial and temporal locations where emissions are expected to occur, with no computed emissions detected in regions where emissions should not exist. To further validate the robustness and applicability of our method, we applied it to the Permian Basin, the largest and fastest-growing oil and gas-producing basin in the United States, located in western Texas and southeastern New Mexico. By aligning our results with known emission source locations in the region, we successfully captured the majority of emission signals, including many smaller emissions that were previously undetected using TROPOMI, thanks to our method's lower detection threshold. Comparisons with conventional approaches, which simply remove negative concentration or emission values, reveal that our method provides a better match with observational data, demonstrating improved stability, accuracy, and a reduction in systematic bias. This highlights that this approach is capable of delivering reliable and precise emission estimates, even in areas with complex sources.

2 Data and Methods

2.1 study data

TROPOMI inverts daily measurements of column-averaged dry-air atmospheric CH₄ column mixing ratio based on a retrieval around the 1.6 and 2.3 μm absorption band, with overpasses occurring daily around 13:30 local time. The XCH₄ retrieval used herein (version 2.4.0 Level-2) relies on a physical algorithm that factors in surface and atmospheric scattering. In this study, we use the methane total column-averaged dry-air mole fraction XCH₄ of TROPOMI from May 2018 to December 2023 in Waliguan (35.5° to 37.1°N latitude, 100.1° to 101.7°E longitude) (Hu et al., 2018; Lorente et al., 2021) and from 2019 to 2020 in the Permian Basin (30° to 33°N latitude, 101° to 105°W longitude). To ensure high quality data, grids with quality assurance less than 0.5 were removed. Swath-by-swath data were resampled day-by-day onto a standard latitude/longitude grid of 0.05° x 0.05° using HARP (<http://stcorp.github.io/harp/doc/html/index.html>).



Wind speed and direction were obtained from the European Centre for Medium-Range Weather Forecasts ERA-5 reanalysis product. Due to the elevation and overpass time, 600hPa levels in the Waliguan area and 875hPa levels in the Permian Basin were selected for meteorology, with the time averages of 13:00 and 14:00 UTC.

Daily ground observations of CH₄ made for more than three decades at Waliguan are obtained from World Data Centre for Greenhouse Gases. The source coordinates and emission rates of methane in the Permian Basin were obtained from an aircraft observational study by Cusworth (2021).

High frequency CH₄ flux was measured nearby a gas extraction vent of a high gas coal mine in Changzhi, Shanxi Province using the eddy correlation method, using CSAT-3 anemometer and LI-7700 and Universal open Path gas analyzer at 10 Hz as published in Hu (2024). The flux was calculated according to the WPL-corrected method (Webb et al., 1980) and subsequently narrowed down to a frequency of every half hour. Observations were made continuously from October 24 to December 21, 2021 and from August 15 to September 13, 2022. The flux observations obtained from eddy covariance observations are specifically used to fit the coefficients of the mass conservation model at the date and time they are available, providing a ground-truth at the place and time the observations were made.

2.2 Mass conservation equation

The method used in this study is based on the continuity equation for conservation of mass of chemical substances in the atmosphere.

$$E = \frac{d}{dt}XCH_4 + H + D + T \quad (1)$$

Where E is the emission flux, $\frac{d}{dt}XCH_4$ is the time derivative of XCH_4 , H is the chemical gain or loss of CH₄, D is the deposition of CH₄, and T is the transport gain or loss of CH₄ on each given grid in space and time. Due to the slow nature of CH₄ loss induced by OH, its low solubility, and its slow removal due to other oxidants and bacteria as compared to the daily-scale observations used herein, the terms for chemical gain H and deposition D in Equation (1) are approximately zero, allowing Equation (1) to be simplified as:

$$\frac{d}{dt}XCH_4 = E - T = E - \alpha * (\nabla \cdot (XCH_4 * U)) - \beta * \nabla \cdot (\nabla XCH_4) \quad (2)$$

The transport term T is approximated by the combination of advection and pressure induced transport $\nabla \cdot (XCH_4 * U)$ and diffusion $\nabla \cdot (\nabla XCH_4)$, where U is wind filed. We specifically use the methane flux measured at Changzhi as E and calculate the time derivative, transport, and diffusion terms for the corresponding position and time over Changzhi. The coefficients α and β are then calculated using Multiple Linear Regression. The resulting emissions have been previously demonstrated to work well in Shanxi (Hu et al, 2024). In this work, the trained model is used to calculate emissions across all grids on all days where there is sufficient available TROPOMI and meteorological data to compute all of the terms.



2.3 Observational Uncertainty Analysis

Our model and other more simplified approaches (Cohen and Prinn 2011; Liu, M et al., 2021; Yu et al., 2023) rely upon concentration gradients, such as the transport term and diffusion term in our equations and the divergence method used by others, when considering a certain volume of air, we can calculate the number of CH₄ molecules flowing into and out of that volume based on column density and representative wind speed and direction acting upon that atmospheric column. Under steady state conditions, a positive difference indicates the presence of a CH₄ emission source. However, the value of a gradient does not linearly vary with the uncertainty in the observations. For instance, if the XCH₄ values at two adjacent grid points are 1800 and 1900 ppb, with a 10% uncertainty, they can range from 1620-1980 ppb and 1710-2190 ppb respectively, leading to a possibility that the gradients could range from negative, to zero, or even moderately positive. Sinks comprise chemical losses, such as reaction with the hydroxyl radical, OH, and atomic chlorine and biological losses, primarily uptake by methanotrophic microbes in soil. The lifetime with respect to reaction with OH in the troposphere is between 10 and 11 years and the average lifetime of methane in the atmosphere is 9 years, methanotrophic bacteria achieved methane oxidation rates of about 5.6 nmol/cm³/day. Forest soils that cover about 30% of the Earth's land surface absorb about 26 to 34 Tg CH₄ per year. However, we calculated TROPOMI XCH₄ data day by day, grid by grid, and the two cases have little effect on methane concentration. Hence, there is no physical means by which a negative lifetime can occur in our framework. Therefore, only white noise generated by the nonlinearity of the concentration gradient is possible to achieve negative emissions.

However, merely removing negative values is not mathematically consistent with white noise, due to the randomness of the uncertainties applied to the observed data being equally likely to be positive or negative. Therefore, any values which fall in the probability distribution which is best fit by a normal distribution with a center at zero, are associated with this noise. They are computed values, but are just due to the noise associated with the observational uncertainty. It is essential to compute how these uncertainties impact the real conditions when considering the spatial change in the observed fields. This includes not only the observed values themselves, but also whether or not the underlying assumptions of the model used are still relevant, or whether the simple idea of a plume model may still be possible. For example, if the gradient switches direction when uncertainty is applied, the chances of the plume being real are significantly reduced, with the original detected plume more likely being just noise, rather than a real signal.

To analyze this effect, we use the mass conservation equation to quantify methane emissions in the area around the Waliguan (WLG) long-term base station, because there are no large known sources of methane emissions in this area, the effect of noise due to the non-linearity of the gradient term can be better demonstrated, with most of the emissions calculated using traditional techniques not computing actual emissions, but rather computing a signal based on observational noise. Two levels of random perturbations are applied to the XCH₄ observations: 10% and 20%. In each case, a respective value ranging from -10% to +10% (or 20% respectively) is made independently to each TROPOMI retrieved XCH₄ data point, day-by-day, and grid-by-grid to simulate realistic and unbiased TROPOMI retrieval errors. 3000 unique sets of perturbations



have been performed. Each of these 3000 data sets have been used to retrain the emissions via equation (2), with the resulting average value grid-by-grid and day-by-day used.

160 2.4 Threshold retrieval

To identify potential emission sources in the study area and separate these from white noise, we take a two-step approach. First, we filter all grids in terms of their mean value, with any grids having temporal average emissions values smaller than the 10th percentile (in this case $21.2 \mu\text{g}/\text{m}^2/\text{s}$) removed, to account for the fact that these grids likely are contributed to exclusively by white noise. Sensitivity tests are performed using different cutoff values for the first cutoff, specifically $17 \mu\text{g}/\text{m}^2/\text{s}$, $25 \mu\text{g}/\text{m}^2/\text{s}$, and $31 \mu\text{g}/\text{m}^2/\text{s}$, and re-computing the resulting emissions each time using all of the TROPOMI uncertainty levels as used elsewhere. Second, the idea is extended to the temporal domain, specifically assuming that any negative emissions values must be uncertain, and therefore any positive value of the same magnitude or smaller is also due to uncertainty. Specifically, within each remaining grid point, the most negative emission value computed is identified $-\theta \mu\text{g}/\text{m}^2/\text{s}$, and all values in the range from $[-\theta: \theta] \mu\text{g}/\text{m}^2/\text{s}$ are then excluded. This filter is applied grid-by-grid basis, since the uncertainty is assumed to be an intrinsic property of each grid point, consistent with how the retrievals are computed. To further validate our method, we applied it to the Permian Basin, comparing our results with strong CH_4 point sources mapped and quantified by Cusworth (2021) using airborne imaging spectrometer technology

3 Results and discussion

3.1 Observation error

175 Due to the following factors, retrievals of CH_4 from TROPOMI may have relatively large uncertainties in some regions (noting that their influence varies as a function of location and time). First, when there is overlap between CH_4 and other species which are not resolved (i.e., waveband resolution of the sensor). Second, when atmospheric conditions reduce incoming solar radiation in the wavebands relevant to CH_4 retrieval (i.e., cloud optical depth and AOD). Third, when atmospheric conditions alter the band-by-band properties of incoming and scattered solar radiation in the wavebands relevant to CH_4 (i.e., BC and CO). Fourth, when changes in the land-surface properties have occurred which are not properly modeled or included, such as due to development, greening, industrial growth, agriculture changes, etc. (i.e., changes in surface reflectivity).

185 The uncertainty of the aerosol products of TROPOMI is 3% to 5% (Torres et al., 2020; Tiwari et al., 2023). As a first order problem, no gas retrievals can be performed until the surface albedo, clouds, and aerosols are first considered (Balasus et al., 2023), or the combination is considered in tandem (Chen et al., 2022). In addition to this point, it has been demonstrated that TROPOMI L2 XCH_4 retrievals are routinely underestimated over regions with high aerosol loadings (K. Li et al., 2024). Therefore, since the region considered has a variable AOD, and one which is quite different from the traditional datasets employed to initiate the inversion algorithm (Liu, Z et al., 2024), therefore this factor must also be



considered in the area being analyzed. For this reason alone, it is not possible for the CH₄ retrieval to have an uncertainty
190 lower than the aerosol retrieval uncertainty. TROPOMI NO₂ has an error range from 10% to 40% or more (Boersma et al.,
2018; Pollard et al., 2022). It is also known that TROPOMI CO has an error range of at least 10% to 20% (Sha et al., 2021).
The uncertainties in the traditional datasets employed with respect to CO over China are significant (Cohen et al., 2025;
Wang et al., 2025). This is important since the CO retrieval is made at the same waveband as the CH₄ retrieval, and therefore
any uncertainty in one product will yield an uncertainty in the other product as previously identified (Gaubert et al., 2016,
195 2017).

The region around Waliguan was specifically selected due to its long-term daily surface observations of CH₄ from 1992
through 2024 (Zhou et al., 2004; Liu, S et al., 2021). Waliguan is the world's highest atmospheric baseline monitoring station
(at 3810 meters) and the only one in the interior of the Northern Hemisphere, making it the best possible representation of a
clean, continental, high atmospheric station in mid-latitudes, and best represents the world's middle atmospheric CH₄ levels.
200 This point is critical, since an outsized number of coal mines with high emissions from China are similarly uniquely located
in Shanxi, Shaanxi, Inner Mongolia, Xinjiang, and other places located at high elevations and far away from the sea (Yang et
al., 2023; Zhang et al., 2020), and is more representative of the conditions under which CH₄ is emitted in China, as well as
some other lesser studied regions around the world (Sadavarte et al., 2021; Hancock et al., 2024). A direct comparison
between the surface observations and the TROPOMI XCH₄ column concentration, as clearly observed in Figure 1b,
205 demonstrates a difference up to 176ppb, or a 9.4% error. Based on this, we add a random perturbation to each retrieved value
of TROPOMI XCH₄ in the range from -10% to 10% to simulate the uncertainty in the retrieval data itself. This is also
consistent with the observational study of (Frankenberg et al., 2016), indicating that the observed error can range over 20%.

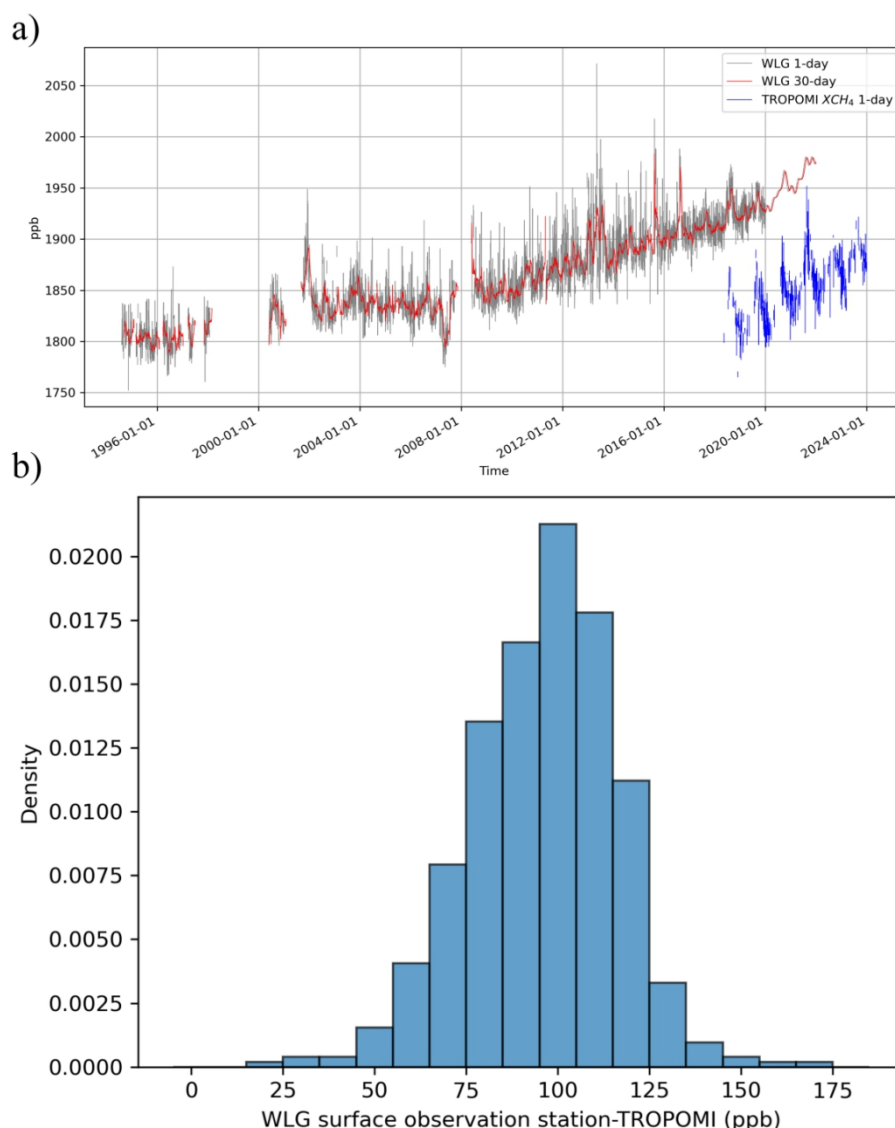


Figure 1: Daily (grey) and 30-day mean (red) methane concentration data from Waliguan from August 1994 to December 2021 and daily series of TROPOMI XCH₄ (blue) from April 2018 to December 2023.

3.2 Comparison of emissions before and after application of filtration in Waliguan area

As illustrated in Figure 2a, the distribution of computed emission over all pixels on all days exhibits a predominantly normal distribution pattern, and therefore closely resembling the distribution of white noise. Upon closer inspection, the distribution reveals a slight positive bias, signifying the presence of mixture of genuine subset of emissions values which are computed not due to the observational uncertainty contained within the overall set of computed emissions data. The distribution derived without employing the two-step filtering process, but incorporating a 10% TROPOMI uncertainty,



shows only marginal deviations from the original emissions. Specifically, 78% of the values fall below the threshold of $21.2 \mu\text{g}/\text{m}^2/\text{s}$, with a minimum of $-85 \mu\text{g}/\text{m}^2/\text{s}$ and a maximum of $88.6 \mu\text{g}/\text{m}^2/\text{s}$.

Figure 2b highlights a significant occurrence of near-zero or negative emissions in spatial regions where no emission sources are expected, suggesting the presence of numerous false positives. To address this, a probability density function (PDF) threshold is established based on the point where the distribution deviates from normality on the positive side. Grids with mean emissions exceeding this threshold are retained to distinguish potential real emissions from noise-dominated grids. An example of such a grid, marked by a black box in Figure 2b, demonstrates a mean emission value surpassing the threshold.

Following this initial spatial filtration, a secondary temporal filtering step is applied to the remaining pixels, with the temporal filtering demonstrated on a specific pixel passing the first filtration test in Figure 2c. This step effectively eliminates unphysical values and those arising solely from observational noise, ensuring that only robust emission estimates are considered for further analysis.

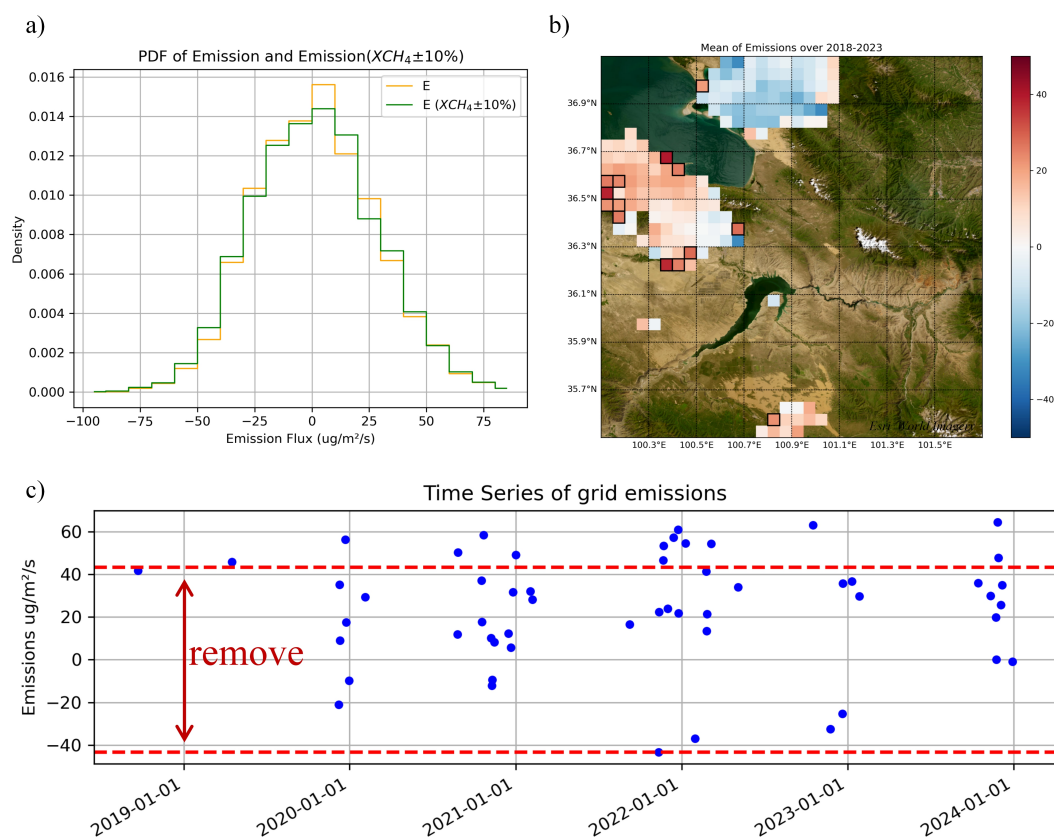


Figure 2: (a) PDF of methane emissions from the Waliguan region calculated using TROPOMI XCH_4 and $XCH_4 \pm 10\%$ based on the mass conservation model; (b) Five-year emission mean calculated by TROPOMI XCH_4 , the mean of the grids in the black



boxes are greater than the set threshold (background portion of image is from Esri World Imagery); (c) The time series of a grid in (b), the emission values between the minimum value and the absolute value of the minimum value in the grid will be removed.

235 The spatial distribution of day-to-day and grid-to-grid emissions over five years is presented in Figure 3a-c (pre-filtering) and Figure 3d-f (post-filtering). A comparison of the filtered emissions in Figure 3d with the actual geographical map reveals that the filtered results accurately capture known emission sources: towns, villages, and shipping docks. These small-scale anthropogenic sources are omitted in existing emission inventories over this region (Crippa et al., 2024). However, our filtering method effectively removes noise, retaining only grid points corresponding to plausible emission
240 sources. All grid points identified as emissions in this study are scientifically justifiable, whereas many grid points initially classified as white noise (Figure 3a) lack any known anthropogenic or natural emission sources substantial enough to have an emission corresponding to the lowest calculated value herein.

The distributions in Figure 3b, e and Figure 3c, f correspond to the 10% and 20% TROPOMI uncertainty scenarios, respectively. These distributions largely overlap with the results shown in Figure 3a and 3d. Specifically, when the
245 TROPOMI XCH₄ data incorporates a 10% error, the filtered grid points align closely with the original emissions, with only a single grid discrepancy. This demonstrates the efficacy of our method in filtering out noise induced by the nonlinearity of the gradient term. However, as the assumed TROPOMI error increases to 20%, the robustness of the filtering method slightly diminishes. Overall, Equation (2) successfully conserves mass by balancing the nonlinearity in the gradient terms through the contributions of other terms, ensuring reliable and consistent results.

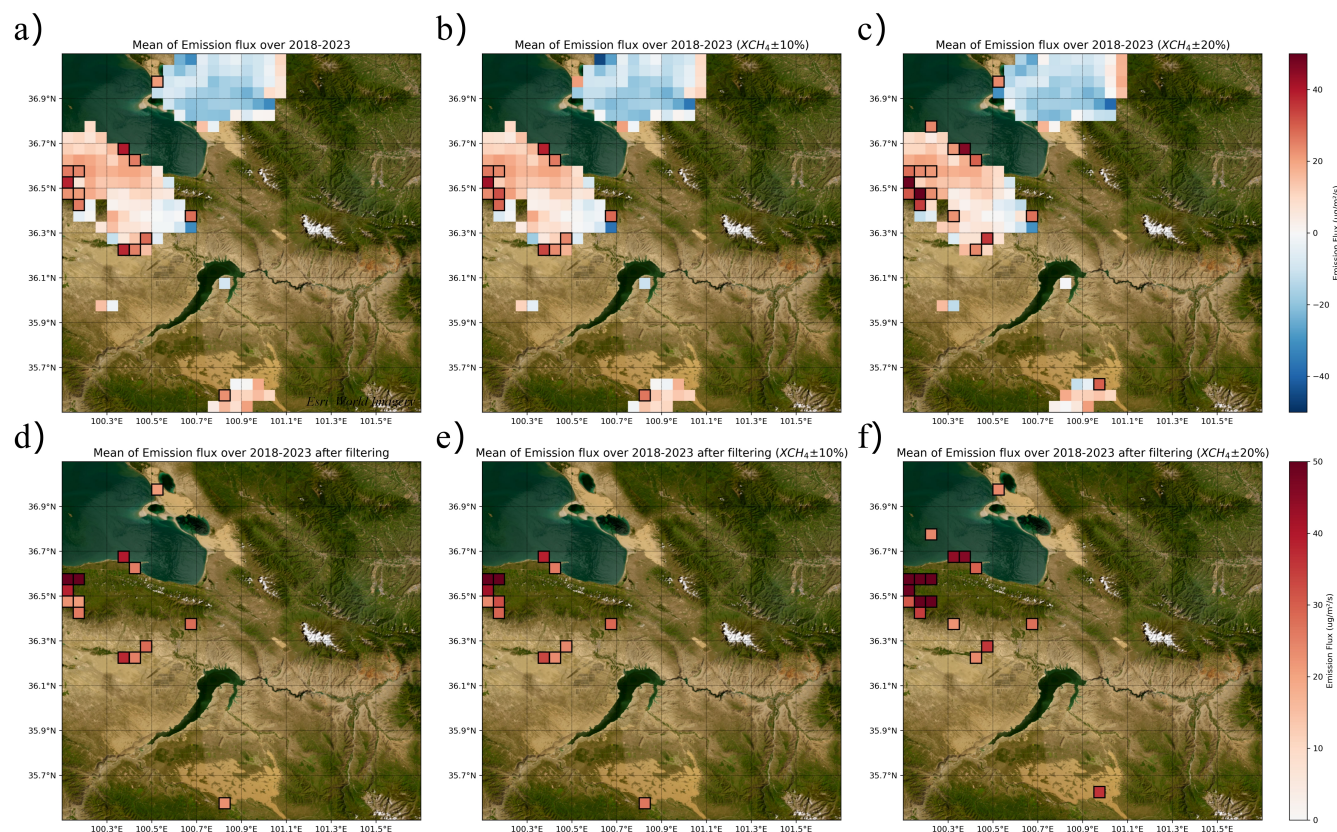


Figure 3: (a), (b), and (c) are maps of five-year emission averages calculated using TROPOMI XCH_4 , $XCH_4 \pm 10\%$, and $XCH_4 \pm 20\%$ respectively; (d), (e) and (f) are maps of the five-year emission average obtained after the two-step filtering is applied corresponding to (a), (b), (c). All backgrounds are from Esri World Imagery.

Scatter plots in Figures 4a and 4b compare the unfiltered emissions with unfiltered 10% and 20% TROPOMI uncertainty emissions, with the respective slope, R^2 statistic, and bias being 1.0, 0.94, 0.14 and 1.0, 0.74, -0.001. The unfiltered emissions contain points which may be mathematically correct, but physically unreasonable including points with a roughly zero mean and substantial noise, or random extreme values. Post two-step filtering results are given respectively in Figures 4c and 4d, and have respective slope, R^2 statistic, bias of 1.05, 0.93, -1.62 and 0.87, 0.6, -6.4. Although the total number of data points is nearly 2 orders of magnitude smaller, the R^2 statistic is similar in the base emissions case and 10% TROPOMI uncertainty case, with an introduced bias of a 5% increase from the original values, which is still within the 10% uncertainty bound. There is a slight reduction in the R^2 in the 20% TROPOMI uncertainty case, with a slightly larger bias of 13% increase from the original values, again still within the 20% uncertainty bound, hinting to the likelihood that a 20% uncertainty in TROPOMI is sufficiently large to bound the nature of the problem in this region of the world.

The range of filtered emissions assuming 0%, 10%, and 20% TROPOMI uncertainty bounds respectively are 1.8-73.8 $\mu\text{g}/\text{m}^2/\text{s}$, 0.5-74.6 $\mu\text{g}/\text{m}^2/\text{s}$, and 10.2-84.6 $\mu\text{g}/\text{m}^2/\text{s}$. In all cases applying the methods herein led to all negative values



(unphysical) being filtered, as well as the largest positive values also being filtered. This is consistent with the fact that some very high observed values are also noise, and that the process herein in fact applies an unbiased and reasonable result. These discrepancies in the mean values arise because the first and second order gradient terms both behave non-linearly when observational uncertainties are included. The fact that the linear terms and the temporal derivative are able to buffer the non-linearity allows the resulting emissions to be robust, and requires that emissions calculations must include these terms to be stable.

Many studies after calculating emission either use an absolute value of the gradient or simply remove negative resulting values, either way retaining only positive results (Maasakkers et al., 2021; Shen et al., 2021; Veefkind et al., 2023; Liu, M et al., 2021). We have performed the same analysis approach and show the results in Figures 4e and 4f to compare the base emissions results against the 10% and 20% TROPOMI uncertainty cases respectively, with the resulting slope, R^2 statistic, and bias of 0.96, 0.87, 0.56 and 0.89, 0.54, -2.44. This method results in emissions that have a less good fit, and include a large amount of noise both near zero as well as some extremely high values at the top. Furthermore, it is found that these extremely high and nearly zero values occur in locations without any known emissions sources. This increase in near-zero noise leads to genuine small emissions sources being indistinguishable from noise, resulting in a lower average emissions per grid, and a far larger number of grids than is realistic.

A sensitivity analysis using different first-step threshold values shows that the resulting values are statistically similar with the slope, R^2 statistic, and bias at $17 \mu\text{g}/\text{m}^2/\text{s}$ (1.00, 0.91, -0.77), $25 \mu\text{g}/\text{m}^2/\text{s}$ (1.05, 0.95, -1.7) and $31 \mu\text{g}/\text{m}^2/\text{s}$ (0.99, 0.94, -1.4) respectively. The only difference is that there are fewer robust datapoints observed in the 20% uncertainty case. Overall, this indicates that the methodology yields results which are relatively robust and stable.

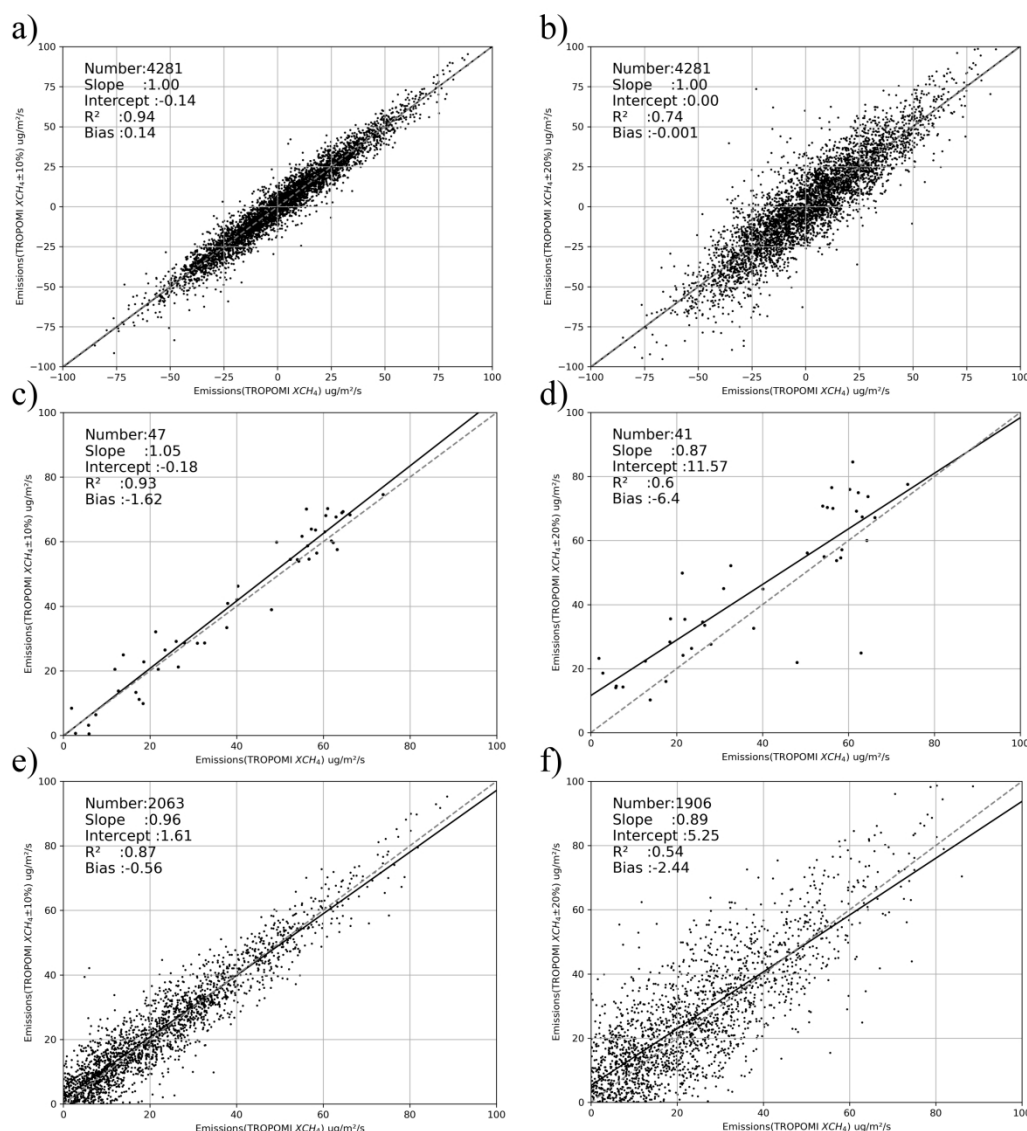


Figure 4: (a), (c), (e) Scatter plots representing each computed emissions value in terms of grid-by-grid and day-by-day from TROPOMI XCH₄ (x-axis) and TROPOMI XCH₄±10% (y-axis); (b), (d), (f) are as (a), (c), (e) respectively, but where the y-axis is TROPOMI XCH₄±20%. Plots (a) and (b) contain all computed emissions before any filtration. Plots (c) and (d) show the results after both thresholds are applied. Plots (e) and (f) apply the traditional method of removing all computed emissions lower than 0 µg/m²/s.

3.3 Methane emissions of the Permian Basin

The Permian Basin, situated in western Texas and southeastern New Mexico, is the largest and fastest-growing oil and gas-producing basin in the United States. According to the U.S. Energy Information Administration (EIA), oil and natural



295 gas production in the Permian Basin surged by 390 percent and 350 percent respectively, from 2014 to 2019. By the end of
2020, the basin accounted for approximately 38 percent of total U.S. oil production and 17 percent of total U.S. natural gas
production. To evaluate the applicability and robustness of our method, we applied the mass conservation equation to
quantify methane emissions in this region from 2019 to 2020.

As depicted in Figure 5a, negative and near-zero values appear in certain areas, with similar results observed when
300 applying divergence-based methods to quantify emissions in this region using TROPOMI with both plume-based methods
(Liu, M et al., 2021; Veeffkind et al., 2022) and chemical transfer models (Shen et al., 2021). The unfiltered computation of
grid-by-grid and day-by-day emissions exhibits a significant positive shift compared to in Waliguan, a reasonable outcome
given the presence of genuine emission signals, but still contains a large amount of data present centered around 0, as evident
in Figure 5b. As previously demonstrated, traditional methods that simply remove negative values or employ background
305 subtraction retain substantial noise near zero and some maxima, leading to artificially low emission estimates.

The results after applying our two-step filtration method are presented in Figure 5c. Post filtration, the mean emission
values are three to four times higher than pre-filtration values, with all negative values and noise near zero effectively
removed. The quantified true emissions range from 0.4 to 218 $\mu\text{g}/\text{m}^2/\text{s}$, with the range of values slightly lower than but
overlapping strong with other studies from substantial coal mining areas in Shanxi China (Hu et al., 2024; Qin et al., 2023).
310 Notably, unlike background subtraction, our filtering method does not indiscriminately remove all values below a
predetermined threshold. As illustrated in Figure 5d, the minimum emission value detected after filtering is 0.4 $\mu\text{g}/\text{m}^2/\text{s}$,
consistent with the smallest detectable signal of 0.5–1.8 $\mu\text{g}/\text{m}^2/\text{s}$ observed in the Waliguan region, demonstrating the
capability of our method to identify small emission signals.

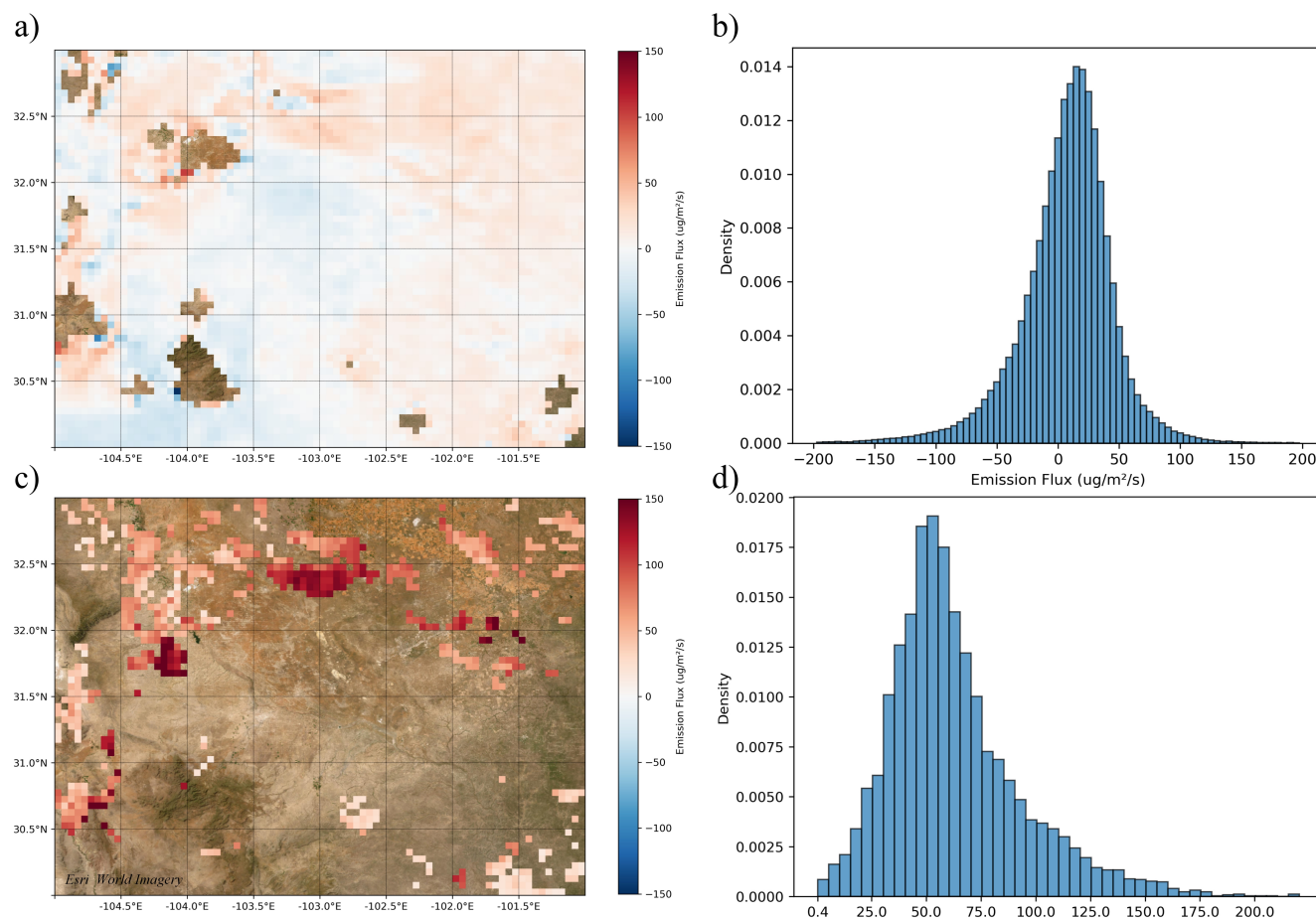


Figure 5: (a) Annual mean methane emission fluxes from the Permian Basin for 2019-2020, (b) PDF of the Permian Basin emission fluxes for 2019-2020, (c) Annual mean methane emission fluxes from the Permian Basin after filtration in 2019-2020, (d) PDF of the 2019-2020 methane emission fluxes from the Permian Basin after filtration. Backgrounds of (a) and (c) are from Esri World Imagery.

To validate our results, we converted the emission fluxes ($\mu\text{g}/\text{m}^2/\text{s}$) into emission rate over each entire TROPOMI grid (kg/h per grid) and compared them with the emission source coordinates and emission rates detected by Cusworth (2021), using airborne imaging spectrometer technology. Cusworth (2021) measured the emission rates of individual sources, and due to the intermittent nature of the aircraft observations, the number of days with detectable emissions varied from 0 to 12 days for each source, with the vast majority having only 1 or 2 days of data. When multiple emission sources were located within a single grid, their emission rates were summed to represent the total emission rate of that grid, as shown in Figure 6a. Given the small sample size of aircraft observations at each point, and the fact that the aircraft observations have a smaller swath width than TROPOMI, we only compare the portion of our emissions distribution grid-by-grid which fall within a one



to three ratio with at least one observed point from the aircraft campaign. The average observation days of each grid are shown in Figure 6c. Figure 6b shows our filtered emission mean, overlapping with the grid of ground emission sources.

330 First, it's clear that our results are larger, which is consistent with the observations made by aircraft having scan widths of 3 and 4.5km, which is always smaller than our grid has a resolution of 0.05 by 0.05, which is about 5km. This means that even if their scan crossed the center of our grid, our grid would still contain information outside of their scan width, and if the scan only crossed a small amount of our grid, then the grid would contain far more information. Second, due to the intermittency of the emission sources, there are zero days of overlap between the two datasets, and hence it is possible that
335 on the day they are measured, some sources may not be emitted, may otherwise be advected into a different direction, may not be detected, or may not be representative of the long time-average emissions. Since our procedure computes far more effective emission days in the region than they do, we opine that the distribution computed it is more likely to represent the real emissions, as shown in Figure 6d. Figures 6e and 6f represent PDFS of ground emission sources and our filtered emissions in an overlapping grid, respectively, Cusworth (2021) observed plume rates across the Permian in the range of 15-
340 16800kg/h, with a maximum value close to ours.

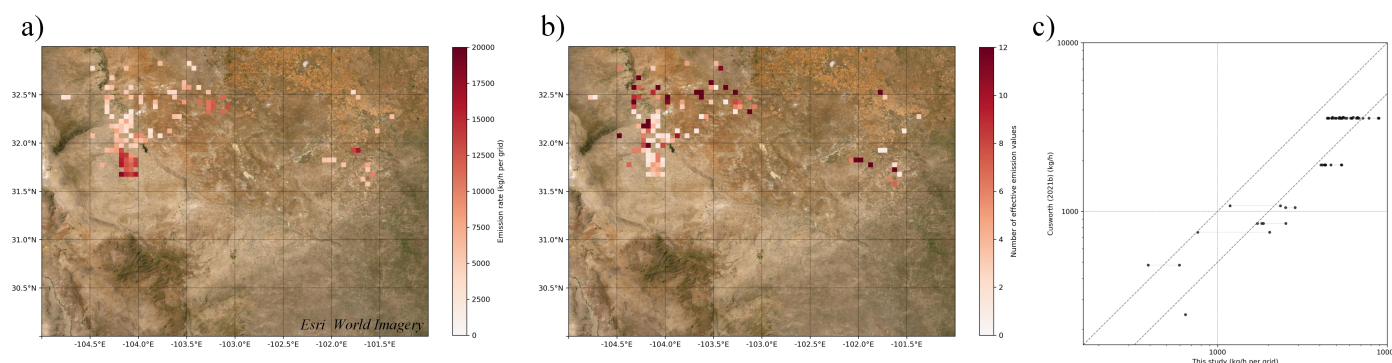


**Figure 6: (a) Annual mean CH₄ emissions (kg/hr/TROPOMI grid) on grids which overlap spatially with an emission observed by observed by Cusworth (2021), (b) Effective days of our filtered emissions, (c) scatter plot representing our emission results and emission values of the ground emission source on overlapping grids, after removing values
345 below 162 kg/h and all data outside of the 1:3 range. Dashed lines represent the 1:1 and 1:2 lines. Backgrounds of (a) and (b) are from Esri World Imagery.**

To further evaluate the consistency between our results and independent observations, on the grids where our results overlap, we display our emission results and the emission values of the ground emission sources respectively, as shown in
350 Figure 6g, after filtering all results from both datasets lower than the minimum detection threshold quantified over Waliguan area of 1.8 $\mu\text{g}/\text{m}^2/\text{s}$ (or 162 kg/h). On a grid-by-grid basis, we have many emission days, and an overall mean emission value larger than the emission source observed on the ground. There is one grid which is larger than ours, 2 grids which are less than 10%, and 4 grids which are less than 20% from the 1:1 line, indicating that the issue of representativeness is a strength of the approach used herein, although an overall reasonable match is obtained from 350kg/hr and up.



355

4. Conclusion

This work used a mass conserving partial differential equation, with terms trained based on observations of CH₄ emissions from Changzhi, Shanxi, to compute emissions of CH₄ using daily and grid-by-grid TROPOMI XCH₄, explicit uncertainty of retrieved XCH₄, and reanalysis meteorological data, over and around the relatively clean area around the long-term WMO CH₄ background observation station at Waliguan and the heavily emitting CH₄ region of the Permian Basin. Inclusion of uncertainty in retrieved TROPOMI XCH₄ values are used to recompute emissions in a manner that considers the physically relevant non-linear effects of gradient calculation. The work further introduced an unbiased two-step filtering method, which effectively removes all negative values as well as both small and larger uncertain values in an unbiased manner, yielding results which are realistic and match well with underlying driving factors.

In Waliguan region we have identified 14 grids which contain CH₄ emissions, with a range from 1.8 to 73.8 µg/m²/s, and validated that all resulting points are all locations containing known anthropogenic CH₄ source activities. The minimum inverted emission value ranges from 0.5 to 1.8 µg/m²/s, depending on the amount of TROPOMI uncertainty applied. The average per-grid and per-day emissions when including an uncertainty of 10% is found to be 5% higher, and when including an uncertainty of 20% is found to be 13% higher, then when not actively considering the TROPOMI retrieval uncertainty. This discrepancy arises due to our model's consideration of both the wind times concentration gradient and second order concentration gradient terms and actively propagates the TROPOMI data uncertainty, requiring a buffering from the linear and temporal derivative terms, a factor overlooked either in the name of model simplification or over-stiffness. When following the typical approach of removing negative emissions or using absolute values, excessive noise near 0 µg/m²/s obscures the true signal, while noisy but large values allow points to enter into the solution space which are also too large to be realistic.

To further validate our approach and results, we compared our emission rates computed over the Permian Basin with aircraft imaging spectrometers estimated by Cusworth (2021). We demonstrated that some results matched within 5%, while the vast majority of the results fell within a 1:2 window. This finding is consistent with the fact that our observations span a longer time series than Cusworth (2021) (more temporally representative) and that the per-grid area is also larger than Cusworth (2021) (per grid possibility of missed sources. This highlights the robustness of our method in capturing both smaller than currently considered possible emissions signals using TROPOMI, as well as reducing some amount of very large emission signals, which likely are a result of TROPOMI inversion noise on the positive side.

This work identifies three weaknesses to be addressed by future work. First, there is need to more carefully consider the inversions of multiple retrieved species in tandem, not just a single species, since other species may impact the inversion of CH₄. Second, future satellite missions which are capable of retrieving XCH₄ at a slightly higher spatial resolution than TROPOMI may yield additional gains. Third, the use of additional platforms that can yield more precise XCH₄ calculations will improve the ability to detect not only more signals, but to widen the possible detection range. Furthermore, there is the issue that the work herein is not reproducing a large number of very small emissions values, as claimed by some works



(Chen et al., 2025), although the results seem to have a lower detection threshold than other TROPOMI based works
390 (Cusworth et al., 2022).

In summary, our method provides a reliable framework for quantifying CH₄ emissions by effectively distinguishing
genuine emission signals from noise, rigorously accounting for observational uncertainties, and validating results against
independent datasets. This represents a significant advancement over traditional approaches, enabling more precise
identification and quantification of CH₄ sources. Importantly, studies relying on TROPOMI or other satellite data that fail to
395 actively incorporate observational uncertainties often underestimate true emissions on a grid-by-grid basis while
simultaneously overestimating the number of emitting grids. This underscores the critical need to integrate uncertainty
propagation into emission quantification methodologies to achieve robust and reliable results.

Data Availability

TROPOMI Level 2 Methane Total Column products are available at
400 https://tropomi.gesdisc.eosdis.nasa.gov/data/S5P_TROPOMI_Level2/S5P_L2_CH4___HiR.2/ from after clicking on the
respective year and day. Daily ground station CH₄ data for Waliguan are obtained World Data Centre for Greenhouse at
<https://gaw.kishou.go.jp/search/file/0013-2015-1002-01-01-9999> after registration. The wind Gases data were obtained from
the European Centre for Medium-Range Weather Forecasts ERA-5 reanalysis product
<https://cds.climate.copernicus.eu/cdsapp#!/dataset/reanalysis-era5-pressure-levels?tab=form> after the precise locations and
405 sought data types are inserted into their platform. The ground measurement data and coefficients of Changzhi coal mine
were obtained from Hu (2024). The point coordinates and emission rates of surface emission sources in the Permian Basin
were obtained from Cusworth (2021). The satellite base maps used in this work are all from Esri World Imagery. All
emissions computed in this work are available for download at private URL <https://figshare.com/s/c653d1ee73147b21a2d8>.
Upon acceptance and publication of the manuscript, these materials will be made publicly available using a permanent
410 figshare doi to ensure reproducibility and to facilitate further research by the scientific community.

Authors contributions

This work was conceptualized by JBC and BZ. The methods were developed by JBC and KQ. LL, WH, PT, SL, AG
and HS provided insights on methodology. Investigation was done by BZ, JBC and KQ. Visualizations were made by BZ
and JBC. Writing of the original draft was done by BZ and JBC. Writing at the review and editing stages were done by BZ
415 and JBC.



Competing interests

The authors declare that they have no conflict of interest.

Acknowledgments

This study was funded by the International Science and Technology Cooperation Program of Jiangsu Province (BZ2024060).

420 The satellite base map used in this study is from Esri World Imagery. These images are used strictly for academic, non-commercial research, in accordance with the fair use policy and in accordance with Eris' Terms of Service.

References

- Balagus, N., Jacob, D. J., Lorente, A., Maasakkers, J. D., Parker, R. J., Boesch, H., Chen, Z., Kelp, M. M., Nesser, H., and Varon, D. J.: A blended TROPOMI+GOSAT satellite data product for atmospheric methane using machine learning to correct retrieval biases, *Atmos. Meas. Tech.*, 16, 3787–3807, <https://doi.org/10.5194/amt-16-3787-2023>, 2023.
- 425 Boersma, K. F., Eskes, H. J., Richter, A., De Smedt, I., Lorente, A., Beirle, S., van Geffen, J. H. G. M., Zara, M., Peters, E., Van Roozendael, M., Wagner, T., Maasakkers, J. D., van der A, R. J., Nightingale, J., De Rudder, A., Irie, H., Pinardi, G., Lambert, J.-C., and Compernelle, S. C.: Improving algorithms and uncertainty estimates for satellite NO₂ retrievals: results from the quality assurance for the essential climate variables (QA4ECV) project, *Atmos. Meas. Tech.*, 11, 6651–6678.
- 430 <https://doi.org/10.5194/amt-11-6651-2018>, 2018.
- Chen, C., Dubovik, O., Schuster, G.L., Chin, Mian., Henze, D. K., Lapyonok, T., Li, Z., Derimian, Y., and Zhang, Y.: Multi-angular polarimetric remote sensing to pinpoint global aerosol absorption and direct radiative forcing, *Nat Commun*, 13, 7459, <https://doi.org/10.1038/s41467-022-35147-y>, 2022.
- Chen, L., Song, Z., Yao, N., Xi, H., Li, J., Gao, P., Chen, Y., Su, H., Sun, Y., Jiang, B., Chen, J., Zhang, Y., Zhu, Y., Li, P., Pang, X., and Yu, S.: Photostationary state assumption seriously underestimates NO_x emissions near large point sources at 10 to 60 m pixel resolution, *Proc. Natl. Acad. Sci.*, 122 (7), e2423915122, <https://doi.org/10.1073/pnas.2423915122>, 2025.
- 435 Cohen, J. B. and Prinn, R. G.: Development of a fast, urban chemistry metamodel for inclusion in global models, *Atmos. Chem. Phys.*, 11, 7629–7656, <https://doi.org/10.5194/acp-11-7629-2011>, 2011.
- Cohen, J. B., Li, X., Pravash, T., Wu, L., Wang, S., He, Q., Yang, H., and Qin, K.: Space-based inversion tracks and attributes Shanxi's under-estimated carbon monoxide emissions, *Research Square* [preprint], <https://doi.org/10.21203/rs.3.rs-4604393/v1>, 16 July 2025.
- 440 Cohen, J. B., Prinn, R. G., and Wang, C.: The impact of detailed urban-scale processing on the composition, distribution, and radiative forcing of anthropogenic aerosols, *Geophysical Research Letters*, 38(10), L10808, <https://doi.org/10.1029/2011GL047417>, 2011.
- 445 Crippa, M., Guizzardi, D., Pagani, F., Schiavina, M., Melchiorri, M., Pisoni, E., Graziosi, F., Muntean, M., Maes, J., Dijkstra, L., Van Damme, M., Clarisse, L., and Coheur, P.: Insights into the spatial distribution of global, national, and subnational greenhouse gas emissions in the Emissions Database for Global Atmospheric Research (EDGAR v8.0), *Earth Syst. Sci. Data*, 16, 2811–2830, <https://doi.org/10.5194/essd-16-2811-2024>, 2024.



- 450 Cusworth, D. H., Duren, R. M., Thorpe, A. K., Olson-Duvall, W., Heckler, J., Chapman, J. W., Eastwood, M. L., Helmlinger, M. C., Green, R. O., Asner, G. P., Dennison, P. E., and Miller, C. E.: Intermittency of Large Methane Emitters in the Permian Basin, *Environ. Sci. Technol. Lett.*, 8, 7, 567–573, <https://doi.org/10.1021/acs.estlett.1c00173>, 2021.
- 455 Cusworth, D. H., Thorpe, A. T., Ayasse, A. K., Stepp, D., Heckler, J., Asner, G. P., Miller, C. E., Yadav, V., Chapman, J. 2., Eastwood, M. L., Green, R. O., Hmiel, B., Lyon, D. R., and Duren, R. M.: Strong methane point sources contribute a disproportionate fraction of total emissions across multiple basins in the United States, *Proc. Natl. Acad. Sci.*, 119 (38), e2202338119, <https://doi.org/10.1073/pnas.2202338119>, 2022.
- de Gouw, J. A., Veefkind, J. P., Roosenbrand, E., Dix, B., Lin, J. C., Landgraf, J., and Levelt, P. F.: Daily Satellite Observations of Methane from Oil and Gas Production Regions in the United States, *Sci Rep.*, 10, 1379, <https://doi.org/10.1038/s41598-020-57678-4>, 2020.
- 460 Erland, B. M., Thorpe, A. K., and Gamon, J. A.: Recent Advances Toward Transparent Methane Emissions Monitoring: A Review, *Environmental Science & Technology*, 56 (23), 16567–16581, <https://doi.org/10.1021/acs.est.2c02136>, 2022.
- Frankenberg, C., Meirink, J. F., Weele, M. V., Platt, U., and Wagner, T.: Assessing Methane Emissions from Global Space-Borne Observations, *Science*, 308, 1010–1014, <https://doi.org/10.1126/science.1106644>, 2005.
- 465 Frankenberg, C., Thorpe, A. K., Thompson, D. R., Hulley, G., Kort, E. A., Vance, N., Borchardt, J., Krings, T., Gerilowski, K., Sweeney, C., Conley, S., Bue, B. D., Aubrey, A. D., Hook, S., and Green, R. O.: Airborne methane remote measurements reveal heavy-tail flux distribution in Four Corners region, *Proc. Natl. Acad. Sci.*, 113(35), 9734–9739, <https://doi.org/10.1073/pnas.1605617113>, 2016.
- Gao, M., Xing, Z., Vollrath, C., Hugenholtz, C. H., and Barchyn, T. E.: Global observational coverage of onshore oil and gas methane sources with TROPOMI, *Sci Rep.*, 13, 16759, <https://doi.org/10.1038/s41598-023-41914-8>, 2023.
- 470 Gaubert, B., Arellano Jr, A. F., Barré, J., Worden, H. M., Emmons, L. K., Tilmes, S., Buchholz, R. R., Vitt, F., Raeder, K., Collins, N., Anderson, J. L., Wiedinmyer, C., Martinez Alonso, S., Edwards, D. P., Andreae, M. O., Hannigan, J. W., Petri, C., Strong, K., and Jones, N.: Toward a chemical reanalysis in a coupled chemistry-climate model: An evaluation of MOPITT CO assimilation and its impact on tropospheric composition, *J. Geophys. Res. Atmos.*, 121, 7310–7343, <https://doi.org/10.1002/2016JD024863>, 2016.
- 475 Gaubert, B., Worden, H. M., Arellano, A. F. J., Emmons, L. K., Tilmes, S., Barré, J., Martinez Alonso, S., Vitt, F., Anderson, J. L., Alkemade, F., Houweling, S., Edwards, D. P.: Chemical feedback from decreasing carbon monoxide emissions, *Geophysical Research Letters*, 44, 9985–9995, <https://doi.org/10.1002/2017GL074987>, 2017.
- Hachmeister, J., Schneising, O., Buchwitz, M., Lorente, A., Borsdorff, T., Burrows, J. P., Notholt, J., and Buschmann, M.: On the influence of underlying elevation data on Sentinel-5 Precursor TROPOMI satellite methane retrievals over Greenland, *Atmos. Meas. Tech.*, 15, 4063–4074, <https://doi.org/10.5194/amt-15-4063-2022>, 2022.
- 480 Hancock, S. E., Jacob, D. J., Chen, Z., Nesser, H., Davitt, A., Varon, D. J., Sulprizio, M. P., Balasus, N., Estrada, L. A., Cazorla, M., Dawidowski, L., Diez, S., East, J. D., Penn, E., Randles, C. A., Worden, J., Aben, I., Parker, R. J., and Maasackers, J. D.: Satellite quantification of methane emissions from South American countries: a high-resolution inversion of TROPOMI and GOSAT observations, *Atmos. Chem. Phys.*, 25, 797–817, <https://doi.org/10.5194/acp-25-797-2025>, 2025.



- 485 He, Q., Qin, K., Cohen, J. B., Li, D.; and Kim, J.: Quantifying Uncertainty in ML-derived Atmosphere Remote Sensing: Hourly Surface NO₂ Estimation with GEMS. *Geophysical Research Letters*, 18(51), e2024GL110468. <https://doi.org/10.1029/2024GL110468>, 2024.
- Hemati, M., Mahdianpari, M., Nassar, R., Shiri, H., and Mohammadimanesh, F.: Urban methane emission monitoring across North America using TROPOMI data: an analytical inversion approach, *Sci Rep*, 14, 9041, <https://doi.org/10.1038/s41598-024-58995-8>, 2024.
- 490 Hu, H., Hasekamp, O., Butz, A., Galli, A., Landgraf, J., Aan de Brugh, J., Borsdorff, T., Scheepmaker, R., and Aben, I.: The operational methane retrieval algorithm for TROPOMI, *Atmos. Meas. Tech*, 9, 5423–5440, <https://doi.org/10.5194/amt-9-5423-2016>, 2016.
- Hu, H., Landgraf, J., Detmers, R., Borsdorff, T., Aan De Brugh, J., Aben, I., Butz, A., and Hasekamp, O.: Toward global mapping of methane with TROPOMI: First results and intersatellite comparison to GOSAT, *Geophysical Research Letters*, 45(8), 3682–3689, <https://doi.org/10.1002/2018GL077259>, 2018.
- 495 Hu, W., Qin, K., Lu, F., Li, D., and Cohen, J. B.: Merging TROPOMI and eddy covariance observations to quantify 5-years of daily CH₄ emissions over coal-mine dominated region, *Int J Coal Sci Technol*, 11, 56, <https://doi.org/10.1007/s40789-024-00700-1>, 2024.
- Li, K., Bai, K., Jiao, P., Chen, H., He, H., Shao, L., Sun, Y., Zheng, Z., Li, R., and Chang, N.: Developing unbiased estimation of atmospheric methane via machine learning and multiobjective programming based on TROPOMI and GOSAT data, *Remote Sensing of Environment*, 304, 114039, <https://doi.org/10.1016/j.rse.2024.114039>, 2024.
- 500 Li, X., Cohen, J. B., Qin, K., Geng, H., Wu, X., Wu, L., Yang, C., Zhang, R., and Zhang, L.: Remotely sensed and surface measurement- derived mass-conserving inversion of daily NO_x emissions and inferred combustion technologies in energy-rich northern China, *Atmos. Chem. Phys*, 23, 8001–8019, <https://doi.org/10.5194/acp-23-8001-2023>, 2023.
- 505 Liang, R., Zhang, Y., Chen, W., Zhang, P., Liu, J., Chen, C., Mao, H., Shen, G., Qu, Z., Chen, Z., Zhou, M., Wang, P., Parker, R. J., Boesch, H., Lorente, A., Maasakkers, J. D., and Aben, I.: East Asian methane emissions inferred from high-resolution inversions of GOSAT and TROPOMI observations: a comparative and evaluative analysis, *Atmos. Chem. Phys*, 23, 8039–8057, <https://doi.org/10.5194/acp-23-8039-2023>, 2023.
- Liu, J., Cohen, J. B., He, Q., Tiwari, P., and Qin, K.: Accounting for NO_x emissions from biomass burning and urbanization doubles existing inventories over South, Southeast and East Asia, *Communications Earth & Environment*, 5, 255, <https://doi.org/10.1038/s43247-024-01424-5>, 2024b.
- 510 Liu, J., Cohen, J. B., Tiwari, P., Liu, Z., Yim, S. H. L., Gupta, P., and Qin, K.: New top-down estimation of daily mass and number column density of black carbon driven by OMI and AERONET observations, *Remote Sensing of Environment*, 315, 114436, <https://doi.org/10.1016/j.rse.2024.114436>, 2024a.
- 515 Liu, M., van der A, R., van Weele, M., Bryan, L., Eskes, H., Veeffkind, P., Liu, Y., Lin, X., de Laat, J., Ding, J.: Current potential of CH₄ emission estimates using TROPOMI in the Middle East, *Atmos. Meas. Tech*, 17, 5261–5277, <https://doi.org/10.5194/amt-17-5261-2024>, 2024.
- Liu, M., van der A, R., van Weele, M., Eskes, H., Lu, X., Veeffkind, P., de Laat, J., Kong, H., Wang, J., Sun, J., Ding, J., Zhao, Y., and Weng, H.: A New Divergence Method to Quantify Methane Emissions Using Observations of Sentinel-5P TROPOMI, *Geophysical Research Letters*, 48(18), e2021GL094151, <https://doi.org/10.1029/2021GL094151>, 2021.
- 520



- Liu, S., Fang, S., Liu, P., Liang, M., Guo, M., and Feng, Z.: Measurement report: Changing characteristics of atmospheric CH₄ in the Tibetan Plateau: records from 1994 to 2019 at the Mount Waliguan station, *Atmos. Chem. Phys.*, 21(1), 393–413, <https://doi.org/10.5194/acp-21-393-2021>, 2021.
- 525 Liu, Z., Cohen, J. B., Wang, S., Wang, X., Tiwari, P., and Qin, K.: Remotely sensed BC columns over rapidly changing Western China show significant decreases in mass and inconsistent changes in number, size, and mixing properties due to policy actions, *npj Clim Atmos Sci*, 7, 124, <https://doi.org/10.1038/s41612-024-00663-9>, 2024.
- Lorente, A., Borsdorff, T., Butz, A., Hasekamp, O., aan de Brugh, J., Schneider, A., Wu, L., Hase, F., Kivi, R., Wunch, D., Pollard, D. F., Shiomi, K., Deutscher, N. M., Velasco, V. A., Roehl, C. M., Wennberg, P. O., Warneke, T., Landgraf, J.: Methane Retrieved from TROPOMI: Improvement of the Data Product and Validation of the First 2 Years of Measurements, *Atmospheric Meas. Tech.*, 14 (1), 665–684, <https://doi.org/10.5194/amt-14-665-2021>, 2021.
- 530 Maasakkers, J. D., Omara, M., Gautam, R., Lorente, A., Pandey, S., Tol, P., Borsdorff, T., Houweling, S., and Aben, I.: Reconstructing and quantifying methane emissions from the full duration of a 38-day natural gas well blowout using space-based observations, *Remote Sensing of Environment*, 270, 112755, <https://doi.org/10.1016/j.rse.2021.112755>, 2021.
- Nesser, H., Jacob, D. J., Maasakkers, J. D., Lorente, A., Chen, Z., Lu, X., Shen, L., Qu, Z., Sulprizio, M. P., Winter, M., Ma, S., Bloom, A. A., Worden, J. R., Stavins, R. N., and Randles, C. A.: High-resolution US methane emissions inferred from an inversion of 2019 TROPOMI satellite data: contributions from individual states, urban areas, and landfills, *Atmos. Chem. Phys.*, 24, 5069–5091, <https://doi.org/10.5194/acp-24-5069-2024>, 2024.
- 535 Parker, P., Boesch, H., Cogan, A., Fraser, A., Feng, L., Palmer, P. I., Messerschmidt, J., Deutscher, N., Griffith, D. W. T., Notholt, J., Wennberg, P. O., and Wuch, D.: Methane observations from the Greenhouse Gases Observing SATellite: Comparison to ground-based TCCON data and model calculations, *Geophysical Research Letter*, 38(15), <https://doi.org/10.1029/2011GL047871>, 2011.
- Pollard, D. F., Hase, F., Sha, M. K., Dubravica, D., Alberti, C., and Smale, D.: Retrievals of XCO₂, XCH₄ and XCO from portable, near-infrared Fourier transform spectrometer solar observations in Antarctica, *Earth Syst. Sci. Data*, 14, 5427–5437, <https://doi.org/10.5194/essd-14-5427-2022>, 2022.
- 545 Prinn, R. G., Huang, J., Weiss, R. F., Cunnold, D. M., Fraser, P. J., Simmonds, P. G., Mcculloch, A., Harth, C., Salameh, P., O’doherly, S., Wang, R. H. J., Porter, L., and Miller, B. R.: Evidence for Substantial Variations of Atmospheric Hydroxyl Radicals in the Past Two Decades, *Science*, 292, 1882–1888, <https://doi.org/10.1126/science.1058673>, 2001.
- Qin, K., Lu, L., Liu, J., He, Q., Shi, J., Deng, W., Wang, S., and Cohen, J. B.: Model-free daily inversion of NO_x emissions using TROPOMI (MCMFE-NO_x) and its uncertainty: Declining regulated emissions and growth of new sources, *Remote Sensing of Environment*, 295, 113720, <https://doi.org/10.1016/j.rse.2023.113720>, 2023
- 550 Qu, Z., Jacob, D. J., Shen, L., Lu, X., Zhang, Y., Scarpelli, T. R., Nesser, H., Sulprizio, M. P., Maasakkers, J. D., Bloom, A. A., Worden, J. R., Parker, R. J., and Delgado, A. L.: Global distribution of methane emissions: a comparative inverse analysis of observations from the TROPOMI and GOSAT satellite instruments, *Atmos. Chem. Phys.*, 21, 14159–14175, <https://doi.org/10.5194/acp-21-14159-2021>, 2021.
- 555 Sadavarte, P., Pandey, S., Maasakkers, J. D., Lorente, A., Borsdorff, T., van der Gon, H. D., Houweling, S., and Aben, I.: Methane Emissions from Superemitting Coal Mines in Australia Quantified Using TROPOMI Satellite Observations, *Environ. Sci. Technol.*, 55, 24, 16573–16580, <https://doi.org/10.1021/acs.est.1c03976>, 2021.



- 560 Schneising, O., Buchwitz, M., Hachmeister, J., Vanselow, S., Reuter, M., Buschmann, M., Bovensmann, H., and Burrows, J. P.: Advances in retrieving XCH₄ and XCO from Sentinel-5 Precursor: improvements in the scientific TROPOMI/WFMD algorithm, *Atmos. Meas. Tech*, 16, 669–694, <https://doi.org/10.5194/amt-16-669-2023>, 2023.
- 565 Sha, M. K., Langerock, B., Blavier, J.-F. L., Blumenstock, T., Borsdorff, T., Buschmann, M., Dehn, A., De Mazière, M., Deutscher, N. M., Feist, D. G., García, O. E., Griffith, D. W. T., Grutter, M., Hannigan, J. W., Hase, F., Heikkinen, P., Hermans, C., Iraci, L. T., Jeseck, P., Jones, N., Kivi, R., Kumps, N., Landgraf, J., Lorente, A., Mahieu, E., Makarova, M. V., Mellqvist, J., Metzger, J.-M., Morino, I., Nagahama, T., Notholt, J., Ohyama, H., Ortega, I., Palm, M., Petri, C., Pollard, D. F., Rettinger, M., Robinson, J., Roche, S., Roehl, C. M., Röhl, A. N., Rousogonous, C., Schneider, M., Shiomi, K., Smale, D., Stremme, W., Strong, K., Sussmann, R., Té, Y., Uchino, O., Velazco, V. A., Vigouroux, C., Vrekoussis, M., Wang, P., Warneke, T., Wizenberg, T., Wunch, D., Yamanouchi, S., Yang, Y., and Zhou, M.: Validation of methane and carbon monoxide from Sentinel-5 Precursor using TCCON and NDACC-IRWG stations, *Atmos. Meas. Tech*, 14, 6249–6304, <https://doi.org/10.5194/amt-14-6249-2021>, 2021.
- 570 Shen, L., Zavala-Araiza, D., Gautam, R., Omara, M., Scarpelli, T., Sheng, J., Sulprizio, M. P., Zhuang, J., Zhang Y., Qu, Z., Lu, X., Hamburg, S. P., and Jacob, D.: Unravelling a large methane emission discrepancy in Mexico using satellite observations, *Remote Sensing of Environment*, 260, 112461, <https://doi.org/10.1016/j.rse.2021.112461>, 2021.
- 575 Tiwari, P., Cohen, J. B., Lu, L., Wang, S., Li, X., Guan, L., Liu, Z., Li, Z., and Qin, K.: Multi-platform observations and constraints reveal overlooked urban sources of black carbon in Xuzhou and Dhaka, *Commun. Earth. Environ*, 6, 38, <https://doi.org/10.1038/s43247-025-02012-x>, 2025.
- Tiwari, P., Cohen, J.B., Wang, X., Wang, S., and Qin, K.: Radiative forcing bias calculation based on COSMO (Core-Shell Mie model Optimization) and AERONET data, *npj Clim Atmos Sci*, 6, 193, <https://doi.org/10.1038/s41612-023-00520-1>, 2023.
- 580 Torres, O., Jethva, H., Ahn, C., Jaross, G., and Loyola, D. G.: TROPOMI aerosol products: evaluation and observations of synoptic-scale carbonaceous aerosol plumes during 2018–2020, *Atmos. Meas. Tech*, 13, 6789–6806, <https://doi.org/10.5194/amt-13-6789-2020>, 2020.
- Vanselow, S., Schneising, O., Buchwitz, M., Reuter, M., Bovensmann, H., Boesch, H., and Burrows, J. P.: Automated detection of regions with persistently enhanced methane concentrations using Sentinel-5 Precursor satellite data, *Atmos. Chem. Phys*, 24, 10441–10473, <https://doi.org/10.5194/acp-24-10441-2024>, 2024.
- 585 Veefkind, J. P., Serrano-Calvo, R., de Gouw, J., Dix, B., Schneising, O., Buchwitz, M., Barré, J., van der A, R. J., Liu, M., and Levelt, P. F.: Widespread frequent methane emissions from the oil and gas industry in the Permian basin, *Journal of Geophysical Research: Atmospheres*, 128, e2022JD037479, <https://doi.org/10.1029/2022JD037479>, 2023.
- Vignati, E., Karl, M., Krol, M., Wilson, J., Stier, P., and Cavalli, F.: Sources of uncertainties in modelling black carbon at the global scale, *Atmos. Chem. Phys*, 10, 2595–2611, <https://doi.org/10.5194/acp-10-2595-2010>, 2010.
- 590 Wang, S., Cohen, J.B., Guan, L., Lu, L., Tiwari, P., and Qin, K.: Observationally constrained global NO_x and CO emissions variability reveals sources which contribute significantly to CO₂ emissions, *npj Clim Atmos Sci*, 8, 87, <https://doi.org/10.1038/s41612-025-00977-2>, 2025.
- Webb, E. K., Pearman, G. I., Leuning, R.: Correction of flux measurements for density effects due to heat and water vapour transfer. *Q J R Meteorol Soc*, 106(447): 85–100, <https://doi.org/10.1002/qj.49710644707>, 1980.



- 595 Yang, G., Zheng, Z., Abbott, B.W., Olefeldt, D., Knoblauch, C., Song, Y., Kang, L., Qin, S., Peng, Y., and Yang, Y.: Characteristics of methane emissions from alpine thermokarst lakes on the Tibetan Plateau, *Nat Commun*, 14, 3121, <https://doi.org/10.1038/s41467-023-38907-6>, 2023.
- Yu, X., Millet, D. B., Henze, D. K., Turner, A. J., Delgado, A. L., Bloom, A. A., and Sheng, J.: A high-resolution satellite-based map of global methane emissions reveals missing wetland, fossil fuel, and monsoon sources, *Atmos. Chem. Phys*, 23, 3325–3346. <https://doi.org/10.5194/acp-23-3325-2023>, 2023.
- 600 Zhang, L., Xia, X., Liu, S., Zhang, S., Li, S., Wang, J., Wang, G., Gao, H., Zhang, Z., Wang, Q., Wen, W., Liu, R., Yang, Z., Stanley, E. H., and Raymond, P. A.: Significant methane ebullition from alpine permafrost rivers on the East Qinghai–Tibet Plateau, *Nat. Geosci*, 13, 349–354, <https://doi.org/10.1038/s41561-020-0571-8>, 2020.
- Zhou, L., Worthy, D. E. J., Lang, P. M., Ernst, M. K., Zhang, X. C., Wen, Y. P., and Li, J. L.: Ten years of atmospheric methane observations at a high elevation site in Western China, *Atmospheric Environment*, 38(40), 7040–7054, <https://doi.org/10.1016/j.atmosenv.2004.02.072>, 2004.
- 605